Vis Comput (2009) 25: 599–607
DOI 10.1007/s00371-009-0349-x

ORIGINAL ARTICLE

Dual-RBF based surface reconstruction

Yuxu Lin · Chun Chen · Mingli Song · Zicheng Liu

Published online: 3 March 2009

Abstract Surface reconstruction (Bloomenthal and Wyvill, Introduction to Implicit Surfaces, 1997) is a fundamental work in Computer Aided Design (CAD) and Computer Graphics (CG). In this paper, motivated by the physical polar field model (Yuxu Lin Chun Chen in Proceedings of the 3rd Pacific-Rim Symposium on Image and Video Technology, 1997), we propose a novel implicit surface reconstruction approach, named Dual-RBF. Through simulating the physical polar field model, Dual-RBF provides a nice initial reconstruction state firstly. Then, two simple nonlinear methods are introduced to adjust the configurations of Dual-RBF model, so that a more accurate reconstruction is reached. Thirdly, the Dual-RBF becomes even more robust to fill the holes on some flawed input point-clouds by adopting a multi-level strategy. Finally, the visualization of the surface reconstruction is speed up with GPU. Experimental results show that the proposed approach is faster and more robust than previous implicit surface reconstruction techniques.

Keywords Dual-RBF · Surface reconstruction · Polar field · GPU

Y. Lin · C. Chen · M. Song (✉)
College of Computer Science, Zhejiang University, Hangzhou, China
e-mail: brooksong@ieee.org

Y. Lin
e-mail: linyuxu@zju.edu.cn

C. Chen
e-mail: chenc@cs.zju.edu.cn

Z. Liu
Microsoft Research, Redmond, USA
e-mail: zliu@microsoft.com

1 Introduction

Implicit surfaces [8, 37] are two-dimensional geometric shapes that exist in three-dimensional space. For their convenient constructive solid geometry and shape blending operations, the implicit surfaces are usually used for compact representation of surfaces in computer graphics and computer-aided design fields. Formally, an implicit surface is defined by $\{x \mid F(x) = 0\}$, we denote it by $F(x) = 0$ for short. So an implicit surface reconstruction problem can be described as following: given a set of scattered points $Q = \{q_i\}$, which is sampled from the original surface, try to reconstruct an implicit surface $F(x) = 0$ which approximates (fits to) the original surface. In the past decades, many researches have been presented to reconstruct implicit surface from scattered points. It is virtually impossible to enumerate all of the previous works on implicit reconstruction. In the literature [8, 13, 15, 35], these previous approaches can be briefly grouped into two categories.

The first group of approaches are based on global fitting, which reconstructs a surface by using a global implicit function, such as polynomial surface [6], "Blooby Model" [27], and radius basis function (RBF) [5, 9, 10, 24, 30, 34], they use relatively simple implicit functions to describe the surface. However, an ideal global fitting on large point-clouds suffers from solving linear system of equations with large matrices (usually not sparse to take advantage of sparse linear solvers [39]) because it is too time consuming. A practical solution is FastRBF [9] which speeds up the solving procedure by centers' reduction and Fast Multipole Method (FMM) [16], but the reconstruction processes are still not fast enough and sometimes fail to preserve the symmetries of the 3D surfaces while input points are too sparse.

The second group of approaches are based on local fitting which overcomes the large scale point-clouds reconstruc-

tion problem. For a local fitting-based approach, it usually approximates local patches with simple implicit functions, then blending these simple implicit functions together as a whole implicit surface [22, 26, 28, 29, 40, 41]. In the work of Ohtake et al. [28, 29], the local patches were approximated by compact supported basis functions or polynomials. And the global implicit surface was obtained by blending them. Alternatively, Alexa et al. [1, 2], Guennebaud et al. [17], and Fleishaman et al. [14] used a moving least square (MLS) projection to approximate the local patches with polynomials. The local fitting-based approaches are usually faster than the global ones. The local fitting approaches, however, often tend to smooth off subtle details and generate artifacts (as shown in Fig. 6) because various of unknown topologies of surfaces cannot be stably captured through small local patches. Very recently, Poisson Surface Reconstruction (PSR) was introduced [20, 21] by treating the surface reconstruction process as a spatial Poisson problem, and the experiments showed that it was also an effective way. But PSR approach can only reconstruct at most $2n$ triangles with n input points, which restricts this method from reconstructing high resolution surfaces from low resolution point-clouds.

From the above reviews we can see that though numerous approaches were presented previously, it is still a challenging work because of the following problems:

(i) the topology of the real surfaces is unknown;
(ii) reconstructing implicit surfaces from large data sets can be inherently expensive due to the computation and memory usage.

Aiming to solve or at least alleviate the mentioned problems and inspired by the physical polar field model, we propose a novel implicit surface reconstruction approach, called Dual-RBF—which utilizes the blending effects of compact support functions to ensure the local smoothness and polar field model to provide accurate reconstructing results. There are several phases in our Dual-RBF implicit surface reconstruction method. Firstly, a nice initial reconstruction state is obtained by simulating the distribution of paired particles in the polar field model locally. Then, a reconstructing process is carried out by minimizing the errors locally. Thirdly, a multi-level strategy is adopted to eliminate the unwanted holes on the surface. Finally, a GPU-based approach is implemented for a faster surface visualization. This paper introduces the following key contributions:

(i) By simulating physical polar field model, a fast and effective Dual-RBF approach is given for 3D point-cloud based surface reconstruction;
(ii) A concept of normalized radial distance is introduce to Dual-RBF reconstruction to adapt the topology of surfaces;
(iii) Two simple nonlinear methods are employed to optimize the particles' configurations locally, which makes the reconstructing process faster than representative local/global reconstruction approaches; and,
(iv) GPU-based approach is adopted to achieve fast Dual-RBF implicit surface visualizing.

The remainder of this paper is organized as follows. In Sect. 2, we give the motivation of the proposed Dural-RBF model. Section 3 details the Dual-RBF model and its estimate, which is the heart of our implicit surface reconstruction method. To eliminate holes on flawed surfaces, we introduce multi-level strategy of our Dual-RBF model in Sect. 4. In Sect. 5, the GPU-based visualization is introduced to get a fast Dual-RBF implicit surface reconstruction. Experimental results and discussion are given in Sect. 6. Conclusion with an outlook to future work is reached in Sect. 7.

2 Motivation

Dual-RBF reconstruction approach is originally motivated by the concept of polar field model [18, 42]. A polar field is generated by two types of particles which have opposite polarities, e.g., electric field and magnetic field. Given locations of particles, their corresponding potential will set up in the field ruled by physical theorem. In [3], polar field was called "indicator field" which was used for repairing problem of triangulations. In [42], the polar field model has been used to reconstruct surfaces by assuming the Gaussian probability distributions of local particles. Motivated by this concept of surface reconstruction, in this paper, with analysis of the relations between surface shapes and particles' configurations, we transfer the surface reconstruction to be a process that estimates the locations and configurations of the particles in a polar field.

For a polar field, the potentials $w^+(r)$ and $w^-(r)$ generated by positive and negative particles respectively have a general form of:

$$w^+(r) = \psi\big(|r|\big), \qquad w^-(r) = -\psi\big(|r|\big) \tag{1}$$

where $|r|$ is the radial distance from the particle, $\psi(.)$ denote a monotonic decreasing function according to $|r|$. As described in [42], a "Parallel-Plate capacitor" model is an instance of the polar field which carries millions of paired particles. As shown in Fig. 1(a), the red and green curves are paralleled conductor plates which carry equal quantity but opposite polarity particles. And the red and green points are positive/negative particles respectively with the normal direction (the arrows) between them. The yellow curve between the positive and negative particles is the insulator which is theoretically infinitely thin. In terms of the potential combination principle in classical physics [18], the potential at a point is the combination of the potentials generated by

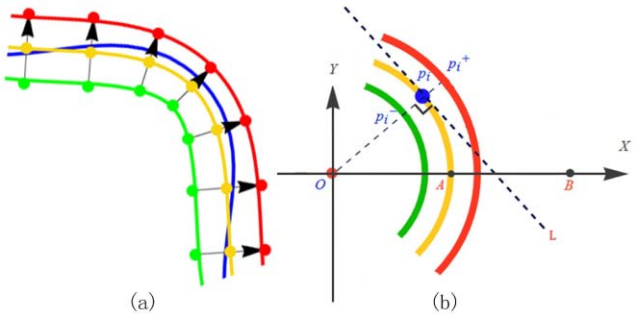

Fig. 1 *From top to bottom*, (**a**) a typical "Parallel-Plate capacitor" model, the *red* and *green curves* are parallel conductor plates which carry equal quantity but opposite polarity particles, the *red* and *green points* are positive/negative particles respectively, the normal direction is from negative particle to positive particle, and the *yellow curve* in the middle is the insulator which separates the two types of particles; (**b**) a local patch of parallel-plate capacitor

all the positive and negative particles. So for a point with location x, its corresponding potential generated by a parallel-plate electric capacitor is:

$$f(x) = \sum_i w_i^+ \left(x - p_i^+\right) + \sum_i w_i^- \left(x - p_i^-\right) \tag{2}$$

where p_i^+ / p_i^- is the location of positive/negative particle; $w_i^+(x - p_i^+)$ and $w_i^-(x - p_i^-)$ are computed in terms of (1).

Figure 1(a) illustrates a zero equipotential curve (blue curve) and its corresponding positive and negative particles. Note that the zero equipotential curve does not coincide with the insulator in practice [18]. For this case, the zero equipotential curve is above the insulator along the direction of curvature, which is caused by the distribution of the positive and negative particles along the insulator. To depict this phenomena clearer, we plot an arbitrary local patch of the capacitor in Fig. 1(b). Without loss of generality, we select an arbitrary point A on the insulator. The direction of the curvature at A is **OA** (coincides with the direction towards/backwards the normal at A) and treated as X-axis. Correspondingly, another point B which is also on the X-axis but far from the origin O is selected. It is obvious that the zero equipotential curve must be above the insulator towards the direction **OA** if the potentials at A and B have opposite signs. To validate this judgment, we choose an arbitrary paired particles p_i^+ / p_i^- whose perpendicular bisector is denoted by L. Because the curve of the insulator is convex near A, A and B lie on opposite sides of L. In other words, A is nearer to p_i^- while B is nearer to p_i^+. Referring to the potential combination principle and taking all the nearby particles into account, the potential at A will be negative and positive at B. Therefore, the potentials at A and B still have opposite sign and the equipotential curve is above the insulator towards the direction of curvature (**OA**).

Inspired by the formation of zero equipotential curve of Parallel-Plate capacitor model, an analogy can be made between Parallel-Plate capacitor model and surface reconstruction problem as follows. Firstly, we regard the equipotential surface (making a straightforward extension of the equipotential curve) as the implicit surface S which we want to reconstruct. The input point-cloud $Q = \{q_i\}$ can be viewed as the sampling points from the equipotential curve. Each sampling point q_i has a corresponding point p_i on insulator. Then, the location of a pair of particles p_i^+ / p_i^- centering at p_i can be inferred, i.e., once we get the location of corresponding points' set $P = \{p_i\}$, the original surface will be fitted to the zero equipotential surface generated by all the particles $P^+ = \{p_i^+\}$ and $P^- = \{p_i^-\}$. Although the locations of $P = \{p_i\}$ on the insulator are unknown, we can initialize them with $p_i = q_i$, and move them toward/backward along the normal direction $N = \{n_i\}$ guide by some energy minimization principle which will be discussed in Sect. 3.2.

3 Dual-RBFs model

The proposed Dual-RBFs model is defined by analogy to the polar field discussed in Sect. 2. In this section, we first introduce the definition of our Dual-RBFs model, then followed by its initialization, finally, two adjustment strategies are employed in our approach to fit the 3D implicit surface accurately.

3.1 Dual-RBFs model and its initialization

3.1.1 Dual-RBF model

For the input point-clouds $Q = \{q_i\}$ sampled from the equipotential curve, their corresponding points on the insulator are denoted by $P = \{p_i\}$ whose locations are initialized as $p_i = q_i$. And the positive/negative particles p_i^+ / p_i^- on each side of the insulator can be inferred by sliding along the normal directions $N = \{n_i\}$ as follows:

$$p_i^+ = p_i + \lambda \cdot n_i \quad \text{and} \quad p_i^- = p_i - \lambda \cdot n_i \tag{3}$$

where λ denotes the particles' offset from the insulator which is set to an extremely small positive value in our approach (0.0001 times of the distance between it and its nearest neighbor) for the insulator is infinitely thin in theory. n_i is the normal of p_i which can be captured by 3D scanner or computed by existing method like in [25], and in our approach, the normals of input points are precomputed with methods proposed in [25].

In order to compute the potential at each point in terms of (1) and (2), it is inevitable to define $\psi(.)$ in advance. In our approach, $\psi(.)$ is defined based on a school of compact support radial basis functions (Gaussian function, B-spline [4], etc.) for their two characteristics: first, compact support radial basis functions have natural smooth blending characteristics; second, their compact support characteristics enable

us to adjust the locations of particles locally at high speed. For instance, we can define $\psi(.)$ as Gaussian function:

$$\psi(r) = e^{-r^2/2\sigma^2}. \tag{4}$$

Taking the positive and the negative particles into account, our radial basis functions appear in pairs. This is why our approach is named "Dual-RBF." Given the definition, it is still difficult to establish the Dual-RBF model based on the point-clouds directly because the input point-clouds are usually not uniformly sampled; i.e., locally for a point p_i, the neighboring particles around it may not distribute uniformly. In some directions, the neighboring points are far from p_i while some are close in other directions. In order to adapt the topology of surfaces, we rewrite $\psi(.)$ by adopting Mahalanobis distance, which still preserves the two characteristics of radial basis functions:

$$\psi(r) = e^{-r^T \cdot \Sigma_i^{-1} \cdot r} \tag{5}$$

where

$$\begin{aligned} \Sigma_i &= \frac{1}{k} \sum_{(p_j \in \text{neighbors of } p_i)} (p_j - c_i)(p_j - c_i)^T \quad \text{and} \\ c_i &= \frac{1}{k} \sum_{(p_j \in \text{neighbors of } p_i)} p_j \end{aligned} \tag{6}$$

where k denotes the number of neighbors to estimate the covariance matrix; in our approach, it is usually set to 20–30, and depends on the requirement of surface smoothness and accuracy (the k nearest neighbors can be obtained very quickly through KD-Tree [33]). From (6), the conventional radial distance is substituted by Mahalanobis distance which normalizes the distance from any direction; that is why we call it normalized radial distance. Taking all the points $P = \{p_i\}$ into account, the global potential function of Dual-RBF model is deduced by integrating (1), (2) and (5):

$$\begin{aligned} f(x) &= \sum_i w_i^+ \left(x - p_i^+\right) + \sum_i w_i^- \left(x - p_i^-\right) \\ w^+(r) &= e^{-r^T \cdot \Sigma_i^{-1} \cdot r} \\ w^-(r) &= -e^{-r^T \cdot \Sigma_i^{-1} \cdot r}. \end{aligned} \tag{7}$$

3.1.2 Dual-RBFs model initialization

The initialization of Dual-RBFs model consists of three steps for the input point-cloud $Q = \{q_i\}$. Firstly, their corresponding points on insulator $P = \{p_i\}$ are initialized as $p_i = q_i$, and the positive/negative particles p_i^+ / p_i^- on each side of the insulator can be inferred by sliding along the normal directions $N = \{n_i\}$ as described in (3); then, for each point p_i, its corresponding covariance matrix Σ_i is computed through (6); thirdly, the global potential function $f(x)$ is obtained by combining the potential functions of all particles in terms of (7); finally, the implicit surface corresponding to the initialized Dual-RBFs model is achieved by setting $f(x) = 0$. Figure 2 shows the reconstructed result from the initialized Dual-RBFs model. The low relative errors of the results (1.6E–4, 4.1E–4 and 1.3E–4) demonstrate that the initialization can give a good beginning for 3D implicit surface reconstruction.

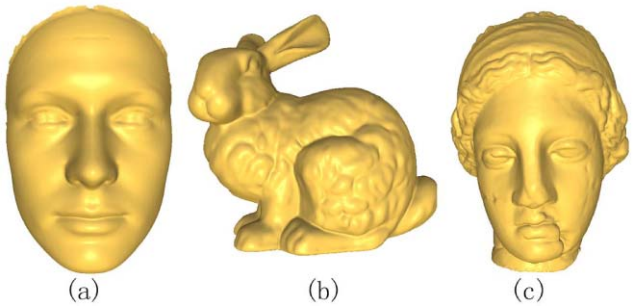

Fig. 2 The initialization reconstruction results, *from left to right*: (**a**) frontal face model with relative error of 1.6E–4; (**b**) bunny model with relative error of 4.1E–4; (**c**) venus model with relative error of 1.3E–4. Note, the input models are listed in Fig. 6

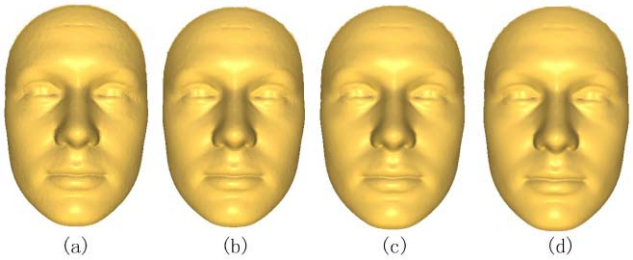

Fig. 3 The initial reconstruction results on different k, *from left to right*: (**a**) $k = 20$, the relative error is 9.48E–5; (**b**) $k = 30$, the relative error is 1.38E–4; (**c**) $k = 40$, the relative error is 1.78E–4; (**d**) $k = 50$, the relative error is 2.16E–4

Considering (6), it is noticeable that the value of k may affect the initialization result because it represents the number of the neighboring particles. In Fig. 3, we plot the initialization reconstruction results with various values of k. It is shown that the relative error increases as k increases, and so does the smoothness.

Note that although the above reconstruction results are just the results of initialized Dual-RBF models without further reconstructing, the relative error is already low enough for many applications, thus providing us with a very nice initial reconstruction state; however, the initial model has not reached the maximum accuracy which Dual-RBF model can do. In the following subsection, two simple nonlinear methods are applied upon this initial Dual-RBF model to get further accuracy, so as to adapt some scenarios which have extremely high accuracy requirement, e.g. feature article of high resolution 3D facial expression.

3.2 Implicit surface reconstruction based on dual-RBFs

For an input point-cloud $Q = \{q_j\}$, an ideal reconstructed implicit surface $f(.) = 0$ should satisfy $f(q_j) = 0$, so, an energy function for Dual-RBF model can be written out as:

$$\begin{aligned} J &= \sum_j f(q_j)^2 \\ &= \sum_j \left(\sum_i w_i^+ (q_j - p_i^+) + \sum_i w_i^- (q_j - p_i^-) \right)^2, \\ p_i^+ &= p_i + \lambda \cdot n_i = q_i + (\lambda + d_i) \cdot n_i, \\ p_i^- &= p_i - \lambda \cdot n_i = q_i + (-\lambda + d_i) \cdot n_i \end{aligned} \tag{8}$$

where $f(q_j)$ is the potential at q_j. The 3D implicit surface reconstruction can be achieved by minimizing the energy function J. However, solving this minimization problem by adjusting the configurations of all paired particles is obviously a nonlinear and time consuming process. Due to the compact support characteristics of the potential function, the potential yielded by the particle-pair p_i^+/p_i^- has a support region which satisfies $e^{-r^T \cdot \Sigma_i^{-1} \cdot r} \leq dmin$, where $dmin$ is the minimal value depending on the computer's precision. Therefore, to adjust the configuration for paired particle p_i^+/p_i^-, only those points that are in the support region of p_i^+/p_i^- involving the computation; therefore, the global nonlinear optimization process is covert to local nonlinear optimization process. In our approach, two simple adjusting strategies are adapted to adjust the configurations of paired-particles locally.

Because we initialize the Dual-RBFs model by setting $p_i = q_i$, which is a straightforward initializing way without any optimization (Sect. 3.1.2), and as Sect. 2 proved, the equipotential curve (with analogy of the initialized reconstruction surface) is above the insulator towards the direction of curvature in this state, to reconstruct more accurate surface, a workable way is to adjust the location of p_i toward/backward along its corresponding normal direction n_i (coinciding with the direction toward/backward the curvature). As we have analyzed, the optimized adjustment d_i for p_i can be computed locally, and quasi-Newton method [31, 32] is employed to solve this energy minimization problem.

The second method is carried out by taking into account of the configuration of the particle pair p_i^+/p_i^-. From (5), the zero equipotential surface yielded by p_i^+/p_i^- with symmetric configuration is always a plane going through p_i, which is in the middle of p_i^+ and p_i^-. However, if we change the configurations of the particle pair to be asymmetric, as below,

$$w^+(r) = e^{-r^T \cdot \Sigma_i^{-1} \cdot r}, \qquad w^-(r) = -e^{-m_i \cdot r^T \cdot \Sigma_i^{-1} \cdot r} \tag{9}$$

where $m_i > 0$ adjusts the normalized radial distance from p_i^-; Σ_i^{-1} is a symmetric positive matrix that can be decomposed through singular value decomposition (SVD) as:

$$\Sigma_i^{-1} = [h, u, v] \cdot \begin{bmatrix} a^2 & 0 & 0 \\ 0 & b^2 & 0 \\ 0 & 0 & c^2 \end{bmatrix} \cdot [h, u, v]^T. \tag{10}$$

Suppose a is the maximum eigenvalue, then its corresponding eigenvector h coincides with the normal at p_i (i.e. $h = n_i$) [25]. Given the eigenvectors, we define a local coordinate space whose axes are h, u and v, and origin is p_i (Fig. 4). In the local coordinate space, $p_i^+ = (\lambda, 0, 0)$, $p_i^- = (-\lambda, 0, 0)$, and zero equipotential surface yielded by p_i^+/p_i^- can be defined $Z = 0$, where:

$$\begin{aligned} Z(h0, u0, v0) = {} & e^{-(a^2 \cdot (h0-\lambda)^2 + b^2 \cdot u0^2 + c^2 \cdot v0^2)} \\ & - e^{-m_i (a^2 \cdot (h0-\lambda)^2 + b^2 \cdot u0^2 + c^2 \cdot v0^2)}. \end{aligned} \tag{11}$$

We further develop $Z = 0$ from (11):

$$\begin{aligned} & a^2 \cdot \left(h0 - \frac{1+m_i}{1-m_i} \lambda \right) + b^2 \cdot u0^2 + c^2 \cdot v0^2 \\ & = a^2 \cdot \lambda^2 \cdot \left(\frac{(1+m_i)^2}{(1-m_i)^2} - 1 \right). \end{aligned} \tag{12}$$

Equation (12) is an ellipsoid function whose intersection points with h axes are: $IT_1 = -\frac{\lambda \cdot (m_i+1)}{m_i - 1}$ and $IT_2 = -\frac{\lambda \cdot (m_i-1)}{m_i+1}$. The zero equipotential surfaces with various m_i are plotted in Fig. 4(a)–(c). It is shown that different values of m_i lead to different sizes of the ellipsoid (infinite when $m_i = 1$). This characteristics enable us to fit the neighboring particles through adjusting the local shape of zero equipotential surface. Like the first adjusting method, the optimized adjustment parameter m_i can also computed by quasi-Newton method [32] local guide by minimizing the energy in (8).

The above two nonlinear adjusting methods are combined in our approach, in other words, there are two parameters equipped with each point p_i : d_i and m_i; in each iteration, we adjust both of them in order (on adjusting one of them, another one is fixed). These adjustments provide a more accurate reconstruction results. The reconstruction results are shown in Fig. 6, the relative error is decreases to 8.22E–6, 8.85E–5 and 2.62E–5 for model "frontal face," "bunny" and "venus"; comparing to the results in Fig. 2, the relative error decreases dramatically (1/10–1/20).

4 Multi-level strategy

Due to the inevitable scanning errors, the input point-cloud often suffers from unwanted holes on the surface. Aiming to carry out 3D implicit surface reconstruction robustly even

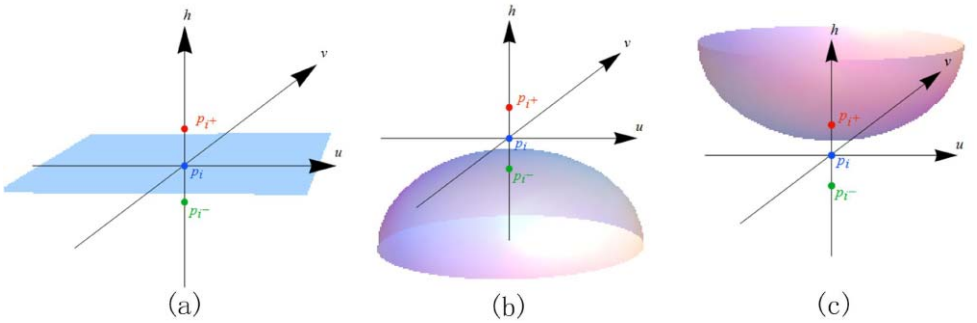

Fig. 4 *From left to right*: (**a**) the zero equipotential surface for $m = 1$; (**b**) the zero equipotential surface for $m > 1$; (**c**) the zero equipotential surface for $m < 1$

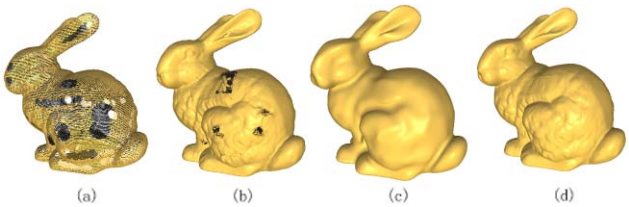

Fig. 5 *From left to right*: (**a**) a bunny model with holes; (**b**) the single level Dual-RBF's reconstruction result; (**c**) the coarse level Dual-RBF's reconstruction result; (**d**) the multi-level Dual-RBF reconstruction result which combines 2 level's potential functions

with the unwanted holes, we utilize the multi-scaling strategy which was widely used in previous surface reconstruction approaches [28, 29, 38].

Firstly, we employ the point-cloud thinning method in [38] to resample the input point-cloud. Several level point-clouds can be obtained, from coarse to fine, denoted by $\{L_j\}$. In our approach, the ratio of the numbers of points between two adjacent levels is set to 0.05–0.1. For each level point-cloud L_j, we apply the Dual-RBFs model to estimate the potential function f^j of this level. Note that the Dual-RBFs model reconstruction on coarse level can reconstruct holes-free surfaces (as shown in Fig. 5(c)). By combining the reconstructed surfaces from coarse to fine, the unwanted holes are eliminated. In our approach, this combination can be simply expressed as the sum of each level's potential functions, i.e., $f(x) = \sum_j f^j(x)$. We compared the single-level Dual-RBF reconstruction result and multi-level Dual-RBF reconstruction result in Fig. 5. It is obvious that the multi-level Dual-RBF is more robust to fill the holes effectively while reserving details.

5 Visualization

It is known that an implicit surface cannot be rendered directly. Polygonization [7, 11, 12, 23, 36], sphere tracing [19], as well as point-based rendering [1], can be used to visualize the implicit surface. In our approach, the support regions of potential function are usually small, so the point-based rendering is more suitable for us to quickly visualize the reconstruction result.

To retrieve high resolution points on a zero equipotential surface, the space is split into many small cubes using octree effectively. Then a binary operation is applied to each cube to detect whether the zero potential surface intersects with the cube. The binary operation is easy to implement, by evaluating the potentials on eight corners of the cube: once there are two corners whose potentials have opposite signs, the binary operation returns true to represent that the intersection happens between the zero equipotential surface and the cube. Finally, the centers of those cubes with true values are collected to act as the high resolution points on the zero-equipotential surface. However, for an $n \times n \times n$ grid, the number of the binary operations is $O(n^3)$. In order to minimize the number of the binary operations, we just take into account those cubes in the support regions of any paired-particles. So only the cubes near the surface are involved and the number of binary operations is decreased to $O(n^2)$.

Moreover, since potential functions are of compact support, Graphics Processing Unit (GPU) based approach is very suitable for retrieving high resolution points on the Dual-RBF surfaces. To carry out our point-based visualization faster, we devise a workflow to adapt the parallel characteristic of GPU. Firstly, we collect those cubes that may intersect with the surface at a specified split depth (eight, in our case). Then, for each of the collected cube, we split it into $5 \times 5 \times 5$ smaller sub-cubes, and the binary operation is performed on each sub-cube to detect whether it intersects with the surface. Finally, those sub-cubes' centers are collected as the high resolution points on the surface. Because of the high parallelism of GPU, those binary operations are computed simultaneously at high speed. We discuss the performance of our visualization approach for experiment evaluation in Sect. 6.

6 Experiments and analysis

The reconstruction experiments are performed on an Intel Q6600 with 2 GBytes ram running windows server 2003. We make comparison with two representative global and local reconstruction approaches: the Fast RBF Toolbox from

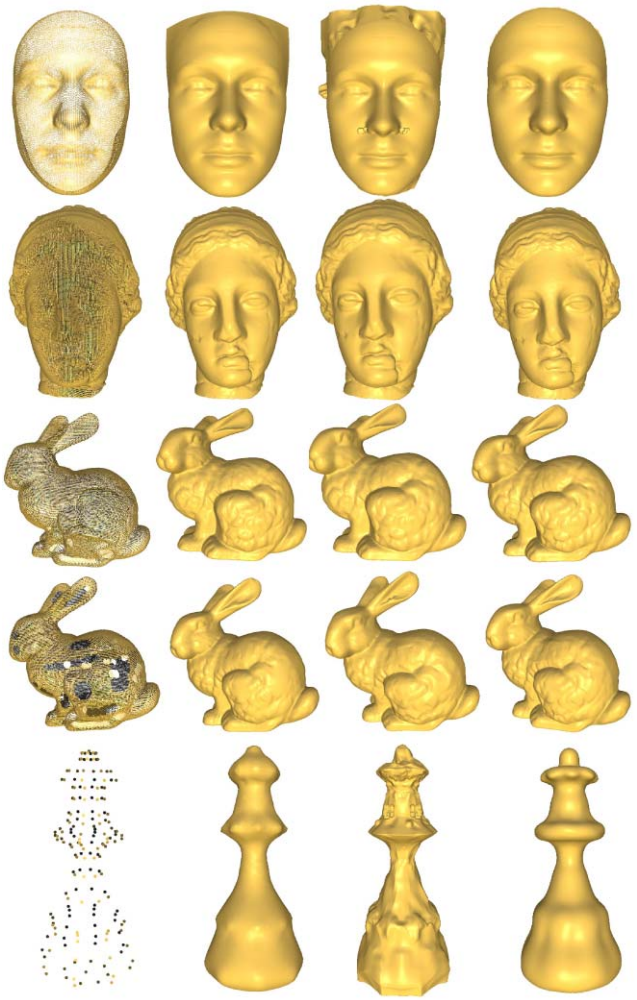

Fig. 6 *From left to right*, in the *first column* is the input model; the *second column* contains the reconstruction results using Fast RBF Toolbox; in the *last column* are the reconstruction results using Dual-RBF. From top to bottom, in the *first row* is frontal face model, the input model consists of 33053 points; in the *second row* is venus model, the input model consists of 134345 points; the *third* input model is bunny model which consists of 34834 points; the *fourth row* is incomplete bunny model, the input model is an incomplete bunny model which consists of 30687 points; the *last row* is a sparse chess model, the input model consists of only 186 points

FarField Technology Ltd. (global one) [9] and the MPU (local one) [28]. For each testing model in our experiments, the diagonal length of the model's bounding box is scaled to 1; the relative error for evaluation is measured by mean square distance between the input points and the reconstructed surface. The parameters are adjusted for each approach until its relative error reaches the threshold. To make the comparison fair, we set relative error threshold for each model. And for better evaluation, the relative error thresholds are set to be small enough but can be reached by the three approaches.

Five models are used in our evaluation. As shown in Fig. 6, the input original models, results from Fast RBF Toolbox, MPU and proposed Dual-RBFs model are listed in columns from left to right. The first input original model in the top row is a frontal 3D face consisting of 33053 points. Both Fast RBF Toolbox and Dual-RBF can produce good results, but MPU produces some extra artifacts near the nose caused by singular fitting at saddle surface. All of the three methods perform well on venus in the second row and bunny in the third row. Even for bunny with holes, Dual-RBFs model can produce more convincible result than the previous methods. However, only the proposed Dual-RBFs model can give good looking result on sparse chess model (186 points). Neither Fast RBF nor MPU can produce acceptable reconstruction as Dual-RBFs model does.

Table 1 The reconstruction time of the three approaches

Model	Relative error threshold	Fast RBF	MPU	Dual-RBF
Face	2E–5	57.6 s	96.3 s	6.32 s
Venus	2E–5	338 s	166 s	44.8 s
Bunny	1E–4	33.6 s	23.7 s	7.05 s
Bunny (incomplete)	2E–4	32.3 s	12.6 s	11.7 s
Chess	2E–3	0.578 s	1.49 s	0.137 s

Time consumption evaluation is also carried out in our experiment. The time consumption is composed by two parts. One part is implicit surface reconstruction and the other is 3D surface visualization. Table 1 shows time consumption of the implicit surface reconstruction. Note that we decrease the relative error threshold for the incomplete bunny, comparing to the original complete one. And for the last sparse chess model, the relative error threshold is adjusted to be higher because of its sparsity. Moreover, it is shown that in most cases, local reconstruction approach (MPU) is faster than global reconstruction approach. And the proposed Dual-RBFs model is even faster than both of them (about 3–16 times faster than Fast RBF Toolbox and MPU).

For the visualization part, as shown in Table 2, given no GPU acceleration, our visualization approach is still faster than FastRBF though slower than MPU. The GPU-based Dual-RBF model is the fastest in most of the cases. And we find that, however, the GPU-based method performs fairly on the sparse model (e.g., chess) since the support regions of its particle pairs are large.

7 Conclusion

In this paper, we present a novel implicit surface reconstruction approach, called Dual-RBF, by analogy of the polar field model. By simulating the classic polar field model, Dual-RBFs model performs initialization, followed by two

Table 2 Comparisons on the visualization time costs and outputs for Fast RBF, MPU and Dual-RBF approaches (CPU and GPU-based), the 'pts' stands for points and 'tris' stands for triangles; for point-based rendering, the outputs are only points. The GPU-based approach is implemented on platform of NVIDIA Geforce 8800GT graphics card and CUDA toolkit

Model	Fast RBF	MPU	Dual-RBF	Dual-RBF (GPU)
Face	189.7 s	47.8 s	110.7 s	15.7 s
	1039K pts	1232K pts	1182K pts	3468K pts
	2073K tris	2461K tris		
Venus	555.3 s	51.8 s	313.5 s	25.9 s
	1577K pts	1166K pts	2013K pts	7232K pts
	3155K tris	2332K tris		
Bunny	215.5 s	42.7 s	211.8 s	17.5 s
	917K pts	1120K pts	2012K pts	3108K pts
	1834K tris	2241K tris		
Bunny	215.2 s	42.2s	207.7s	36.1 s
(incomplete)	921K pts	1122K pts	2025K pts	3501K pts
	1842K tris	2245K tris		
Chess	0.203 s	11.5 s	8.28 s	6.23 s
	3.45K pts	456K pts	213K pts	1071K pts
	6.88K tris	912K tris		

nonlinear adjustments for higher accuracy. Multi-level strategy is adopted to carry out the implicit surface reconstruction robustly. The experimental results show that the proposed Dual-RBFs model is robust to very sparse models and models with holes. Moreover, both the reconstruction and the visualization processes of Dual-RBFs model are much faster than the two existing representative local and global approaches.

In the future, we intend to pay more effort on GPU-based implementation of the whole implicit surface reconstruction process. And more efficient hole detection in the multilevel strategy will also be explored in our future work.

References

1. Alexa, M., Behr, J., Cohen-Or, D., Fleishman, S., Levin, D., Silva, C.: Computing and rendering point set surfaces. IEEE Trans. Vis. Comput. Graph. **9**(1), 3–15 (2003)
2. Alexa, M., Behr, J., Cohen-Or, D., Fleishman, S., Levin, D., Silva, C.T.: Point set surfaces. In: Proceedings of the Conference on Visualization '01, pp. 21–28. IEEE Computer Society, Washington (2001)
3. Alexander, E., Vaclav, S.: A method for repairing triangulations. In: Proceedings of International Conference Graphicon, Moscow, Russia (2004)
4. Bartels, R.H., Beatty, J.C., Barsky, B.A.: An Introduction to Splines for Use in Computer Graphics & Geometric Modeling. Morgan Kaufmann, San Francisco (1987)
5. Beatson, R., Cherrie, J., Mouat, C.: Fast fitting of radial basis functions: methods based on preconditioned GMRES iteration. In: Advances in Computational Mathematics, vol. 11, pp. 253–270. Springer, Berlin (1999)
6. Blane, M.M., Lei, Z., Çivi, H., Cooper, D.B.: The 3l algorithm for fitting implicit polynomial curves and surfaces to data. IEEE Trans. Pattern Anal. Mach. Intell. **22**(3), 298–313 (2000)
7. Bloomenthal, J.: An implicit surface polygonizer. Graph. Gems IV **1**, 324–349 (1994)
8. Bloomenthal, J., Wyvill, B. (eds.): Introduction to Implicit Surfaces. Morgan Kaufmann, San Francisco (1997)
9. Carr, J.C., Beatson, R.K., Cherrie, J.B., Mitchell, T.J., Fright, W.R., McCallum, B.C., Evans, T.R.: Reconstruction and representation of 3d objects with radial basis functions. In: Proceedings of the 28th Annual Conference on Computer Graphics and Interactive Techniques, pp. 67–76. ACM, New York (2001)
10. Carr, J.C., Beatson, R.K., McCallum, B.C., Fright, W.R., McLennan, T.J., Mitchell, T.J.: Smooth surface reconstruction from noisy range data. In: Proceedings of the 1st International Conference on Computer Graphics and Interactive Techniques in Australasia and South East Asia, pp. 119–126. ACM, New York (2003)
11. Cermak, M., Skala, V.: Polygonization of implicit surfaces with sharp features by edge-spinning. Vis. Comput. **21**(4), 252–264 (2005)
12. Cermak, M., Skala, V.: Polygonisation of disjoint implicit surfaces by the adaptive edge spinning algorithm of implicit objects. Int. J. Comput. Sci. Eng. **3**(1), 45–52 (2007)
13. Dierckx, P.: Curve and Surface Fitting with Splines. Oxford University Press, Oxford (1993)
14. Fleishman, S., Cohen-Or, D., Alexa, M., Silva, C.T.: Progressive point set surfaces. ACM Trans. Graph. **22**(4), 997–1011 (2003)
15. Floater, M.S., Hormann, K.: Surface parameterization: a tutorial and survey. Adv. Multiresolut. Geom. Model. **1**, 157–186 (2005)
16. Greengard, L., Rokhlin, V.: A fast algorithm for particle simulations. J. Comput. Phys. **73**(2), 325–348 (1987)
17. Guennebaud, G., Gross, M.: Algebraic point set surfaces. In: ACM SIGGRAPH 2007 Papers, p. 23. ACM, New York (2007)
18. Halliday, D., Resnick, R., Krane, K.: Physics. Wiley, New York (2002)
19. Hart, J.: Sphere tracing: a geometric method for the antialiased ray tracing of implicit surfaces. Vis. Comput. **12**(10), 527–545 (1996)
20. Hoppe, H.: Poisson surface reconstruction and its applications. In: Proceedings of the 2008 ACM Symposium on Solid and Physical Modeling, p. 10. ACM, New York (2008)
21. Kazhdan, M., Bolitho, M., Hoppe, H.: Poisson surface reconstruction. In: Proceedings of the Fourth Eurographics Symposium on Geometry Processing, pp. 61–70. Eurographics Association, Aire-la-Ville (2006)
22. Kitago, M., Gopi, M.: Efficient and prioritized point subsampling for csrbf compression. In: Symposium on Point-Based Graphics, Eurographics (2006)
23. Lewiner, T., Lopes, H., Vieira, A., Tavares, G.: Efficient implementation of marching cubes' cases with topological guarantees. J. Graph. Tools **8**(2), 1–16 (2003)
24. Li, Q., Wills, D., Phillips, R., Viant, W., Griffiths, J., Ward, J.: Implicit fitting using radial basis functions with ellipsoid constraint. Comput. Graph. Forum **23**(1), 55–69 (2004)
25. Mitra, N.J., Nguyen, A.: Estimating surface normals in noisy point-cloud data. In: Proceedings of the Nineteenth Annual Symposium on Computational Geometry, pp. 322–328. ACM, New York (2003)
26. Morse, B.S., Yoo, T.S., Rheingans, P., Chen, D.T., Subramanian, K.R.: Interpolating implicit surfaces from scattered surface data using compactly supported radial basis functions. In: ACM SIGGRAPH 2005 Courses, p. 78. ACM, New York (2005)
27. Muraki, S.: Volumetric shape description of range data using "blobby model". In: Proceedings of the 18th Annual Conference on Computer Graphics and Interactive Techniques, pp. 227–235. ACM, New York (1991)
28. Ohtake, Y., Belyaev, A., Alexa, M., Turk, G., Seidel, H.P.: Multi-level partition of unity implicits. In: ACM SIGGRAPH 2003 Papers, pp. 463–470. ACM, New York (2003)

29. Ohtake, Y., Belyaev, A., Seidel, H.P.: A multi-scale approach to 3d scattered data interpolation with compactly supported basis functions. In: Proceedings of the Shape Modeling International 2003, p. 292. IEEE Computer Society, Washington (2003)
30. Pan, R., Skala, V.: Implicit surface modeling suitable for inside/outside tests with radial basis functions. In: 10th IEEE International Conference on Computer-Aided Design and Computer Graphics, pp. 28–28 (2007)
31. Press, W., Teukolsky, S., Vetterling, W., Flannery, B.: Numerical Recipes in C: The Art of Scientific Computation. Cambridge University Press, Cambridge (1992)
32. Press, W., Teukolsky, S., Vetterling, W., Flannery, B.: Numerical Recipes in C++. Cambridge University Press, Cambridge (2002)
33. Samet, H.: The Design and Analysis of Spatial data Structures. Addison-Wesley Longman, Boston (1990)
34. Samozino, M., Alexa, M., Alliez, P., Yvinec, M.: Reconstruction with Voronoi centered radial basis functions. In: SGP '06: Proceedings of the Fourth Eurographics Symposium on Geometry Processing, pp. 51–60. Eurographics Association, Aire-la-Ville (2006)
35. Schall, O., Samozino, M.: Surface from scattered points: A brief survey of recent developments. In: Proceedings of 1st International Workshop on Semantic Virtual Environments, pp. 138–147. Villars sur Ollon, Switzerland (2005)
36. Schroeder, W., Martin, K.M., Lorensen, W.E.: The Visualization Toolkit (2nd ed.): An Object-Oriented Approach to 3D Graphics. Prentice-Hall, Upper Saddle River (1998)
37. Taubin, G.: Estimation of planar curves, surfaces, and nonplanar space curves defined by implicit equations with applications to edge and range image segmentation. IEEE Trans. Pattern Anal. Mach. Intell. **13**(11), 1115–1138 (1991)
38. Tobor, I., Reuter, P., Schlick, C.: Multi-scale reconstruction of implicit surfaces with attributes from large unorganized point sets. In: Proceedings of the Shape Modeling International 2004, pp. 19–30. IEEE Computer Society, Washington (2004)
39. Toledo, S.: Taucs: A library of sparse linear solvers, version 2.2. Tel-Aviv University. Available online at http://www.tau.ac.il/stoledo/taucs (2003)
40. Walder, C., Scholkopf, B., Chapelle, O.: Implicit surface modelling with a globally regularised basis of compact support. In: Computer Graphics Forum, vol. 25, pp. 635–644. Blackwell Synergy, Oxford (2006)
41. Walder, C., Scholkopf, B., Chapelle, O.: Implicit surface modelling with a globally regularised basis of compact support. Tech. rep., Max Planck Institute for Biological Cybernetics, Department of Empirical Inference, Tübingen, Germany (2006)
42. Yuxu Lin Chun Chen, M.S.J.B.Z.L.: Implicit surface reconstruction with an analogy of polar field model. In: Proceedings of the 3rd Pacific-Rim Symposium on Image and Video Technology, Tokyo, Japan (2009)

Yuxu Lin is a Ph.D. candidate in Microsoft Visual Perception Laboratory, Zhejiang University. His research interests mainly include 3D face modeling and deformation. He is a member of IEEE.

Chun Chen is a Professor in the College of Computer Science, Zhejiang University. His research interests include computer vision, computer graphics and embedded technology.

Mingli Song is a researcher in Microsoft Visual Perception Laboratory, Zhejiang University. He received the Ph.D. degree in Computer Science from Zhejiang University, China, in 2006. His research interests include face modeling and facial expression analysis. He is a member of the IEEE.

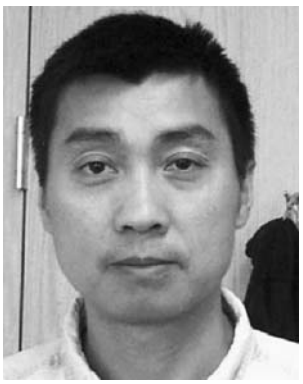

Zicheng Liu received the Ph.D. degree in Computer Science from Princeton University, the M.Sc. degree in Operational Research from the Institute of Applied Mathematics, Chinese Academy of Sciences, Beijing, China, and the B.Sc. degree in Mathematics from Huazhong Normal University, Wuhan, China. He is currently a researcher at Microsoft Research. Before joining Microsoft, he worked as a member of technical staff at Silicon Graphics focusing on trimmed NURBS tessellation for CAD model visualization. His research interests include 3D face modeling and facial animation, linked Bgure animation, multisensory speech enhancement, and multimedia signal processing. He was the Co-chair of the IEEE International Workshop on Multimedia Technologies in E-Learning and Collaboration in 2003. He is a senior member of the IEEE.